Optical and Physical Properties of Cobalt Oxide Films Electrogenerated in Bicarbonate Aqueous Media

Danick Gallant,[†,‡] Michel Pézolet,[†] and Stéphan Simard*[,†,‡]

Département de chimie, Université Laval, Québec (Québec), Canada G1K 7P4, and Département de biologie, chimie et sciences de la santé, Université du Québec à Rimouski, 300, Allée des Ursulines, Rimouski (Québec), Canada G5L 3A1

Received: November 18, 2005; In Final Form: January 27, 2006

For the first time, cobalt oxide films that are highly protective against localized corrosion and depicting a wide variety of bright and uniform colors due to light interference, have been successfully electrogenerated on polycrystalline cobalt disk electrodes under potentiostatic polarization in a mild aqueous bicarbonate medium. Open circuit potential measurements have shown the formation of a film with a bilayered structure, organized as a thin Co_3O_4 outer layer and a thick CoO inner layer. The existence of Co_3O_4 as a thin outer layer, previously postulated from galvanostatic reduction experiments, has been confirmed from XPS analysis. Raman spectroscopy, performed using a very low laser intensity, has shown that the films are mainly composed of CoO. The broadness of the Raman bands observed is associated to the amorphous character of the film, a result that has been confirmed by spectroscopic ellipsometry and X-ray diffraction analysis. Overall film thicknesses, well controlled by the anodization duration, were determined and correlated using mechanical (atomic force microscopy and profilometry) and spectroscopic (specular UV−vis−NIR reflectance and ellipsometry) techniques. Spectroscopic ellipsometry, using a simple *amorphous* dispersion model, has proved efficient for measuring thicknesses of films ranging from 31 to 290 nm with very low standard deviations. The real part of the complex refractive indices of these films, ranging from 1.8 to 2.2 (at $\lambda = 632.8$ nm) depending on the anodization duration, is in good agreement with values reported in the literature for CoO. The film with the highest refractive index, and consequently the more densely packed structure, was obtained following a 30-minute anodization period.

Introduction

Cobalt oxides CoO and Co_3O_4, which are well known to be the stable oxides in the Co−O system,[1−4] present many interesting electronic and magnetic properties which make them efficient catalysts in a wide variety of reactions.[5,6] They are recognized for their promising applications in scientific and technological fields,[7] and are classified as one of the most versatile oxide materials among the transition metal oxides.[3] Recently, various preparation procedures have been reported for cobalt oxide films, such as spray pyrolysis methods, electrodeposition, oxidation of cobalt, thermal decomposition of an aqueous or organic solution of cobalt nitrate, or dip coating processes.[1−3,8]

In a recent paper,[9] we reported a new, simple procedure to electrogenerate cobalt oxide films on a rotating cobalt disk electrode (RDE) under particularly mild experimental conditions. It was clearly demonstrated that these films display, under anodic polarization, a highly protective character against localized corrosion induced by chloride ions in aqueous media. This main property can eventually make these new films good candidates for the preparation of protective coatings for industrial cobalt alloys. Studies on the protection of cobalt and its alloys by anodization are of great interest since cobalt-based coatings are good replacement materials for electroplated hard chrome.[10] Recently, we have found that the novel electrochemical procedure presented,[9] which requires the application of an unusually low electrical potential, produces cobalt oxide films showing a variety of bright colors. To the best of our knowledge, despite the fact that many papers have reported the electrochromic properties of cobalt oxides,[6,11−18] none of these studies describes a method for the preparation of cobalt oxide films that exhibit an assortment of uniform colors due to iridescence. Moreover, the convenient preparation method proposed in the present paper has the unique advantage over other existing techniques of requiring very low-cost materials and of generating uniform cobalt oxide films with outstanding efficient anticorrosive properties, as well as very easily reproducible physical and optical characteristics. This paper reports a complete and fundamental investigation of the optical and physical properties of new, well-structured, brightly colored and protective electrogenerated cobalt oxide films on polycrystalline cobalt substrate under very mild experimental conditions.

Experimental Details

Electrochemical Experiments. Oxide films were electrogenerated on one side of a removable (for further ex situ analysis) polycrystalline cobalt disk (99.95%; $d = 12.0$ mm; thickness = 2 mm), properly mounted and sealed on an aluminum rotating holder that ensures the electrical contact. The auxiliary electrode was a platinized platinum foil separated from the main compartment by a Nafion membrane. The reference electrode was a saturated calomel electrode (SCE) connected

* Corresponding author. E-mail: stephan_simard@uqar.qc.ca. Phone: 418-723-1986 ext. 1488. Fax: 418-724-1849.
† Université Laval.
‡ Université du Québec à Rimouski.

10.1021/jp056689h CCC: $33.50
Published on Web 03/14/2006

to the cell by a bridge and a Luggin capillary. All potentials given below are referenced to this electrode. The volume of the electrochemical cell was 0.5 L, so that the concentration of dissolved cobalt in the bulk can be neglected.

The colored films were electrogenerated on rotating (1000 rpm) cobalt disks during potentiostatic experiments by a polarization at a potential of 0.15 V for different durations, ranging from 5 to 60 min. The electrolyte was an aqueous 0.4 M $NaHCO_3$ solution at pH 8.9. The pH value was reached by adding small volumes of a concentrated NaOH solution to the freshly prepared bicarbonate solution, and maintained stable and free of dissolved oxygen by bubbling a mixture of 500 mL min^{-1} N_2 and 7 mL min^{-1} CO_2. The electrode surface was successively ground with 600 and 1200 grit emery papers and mechanically polished with 5.0, 1.0, and 0.05 μm alumina suspensions, and rinsed with deionized water before each immersion. At the beginning of each experiment, the electrode potential was held at -1.05 V for four minutes to obtain an oxide-free surface. Aqueous solutions were prepared using A.C.S. grade chemicals and deionized water. All experiments were performed at a controlled temperature of 22 °C. Electrochemical experiments were performed with a PAR 263-2A potentiostat and a Pine bipotentiostat model AFCBP1. The electrode rotator was a Pine analytical rotator model AFSAR.

Film Characterization. The Raman spectra of films and standards were obtained during a 120 s acquisition time with a Horiba Jobin-Yvon model LabRam HR800 Raman spectrometer with a Peltier-cooled CCD detector. Excitation was achieved using the 514.54 nm line of an Innova 70C (Coherent) laser. The laser was focused on a $d \approx 1$ μm spot using a BX 40 Olympus microscope with an objective lens of 100× magnification, and backscattered Raman light was efficiently collected by the same lens. The intensity of the laser beam was controlled using appropriate neutral density filters. Ellipsometry spectra of cobalt substrate and films were obtained with an Horiba Jobin-Yvon model UVISEL ellipsometer. A Xe lamp was used as a light source, and the spectra were recorded in the wavelength range of 300 to 1000 nm. The incidence angle was 70°. UV−vis−NIR specular reflectance spectra were recorded using a Varian UV−vis−NIR Cary 500 spectrophotometer. The incidence angle was 22°. Profilometry results were obtained using a Dektak profilometer, having a vertical resolution of 10 angstroms. Atomic force microscopy measurements were performed in the tapping mode of a Multimode atomic force microscope model MMAFM-2 from Digital Instruments (Veeco Metrology Group). The scanning electron microscopy (SEM) images were obtained with a scanning electron microscope JEOL model JSM-6460LV under high vacuum conditions. The X-ray photoelectron spectra (XPS) were taken using the Mg Kα photon source ($h\nu = 1253.6$ eV) of a Kratos Analytical model Axis-Ultra spectrometer. The binding energies were calibrated with peaks Au $4f_{7/2}$ at 83.95 eV, Ag $3d_{5/2}$ at 368.20 eV, and Cu $2p_{3/2}$ at 932.60 eV.

Results and Discussion

1. Electrogeneration of a Bilayered Film on Cobalt RDE. Figure 1 shows the cyclic voltammetry trace for a cobalt RDE in a 0.4 M $NaHCO_3$ solution at pH 8.9. The potential applied for the cobalt oxide production (i.e., 0.15 V) is located in the transition region between the first and the secondary passivation zones. From the results of electrochemical experiments and thermodynamic data, this transition region has already been identified as being favorable for CoO and/or Co_3O_4 formation in bicarbonate[19−21] or borate[22,23] buffers. Moreover, several

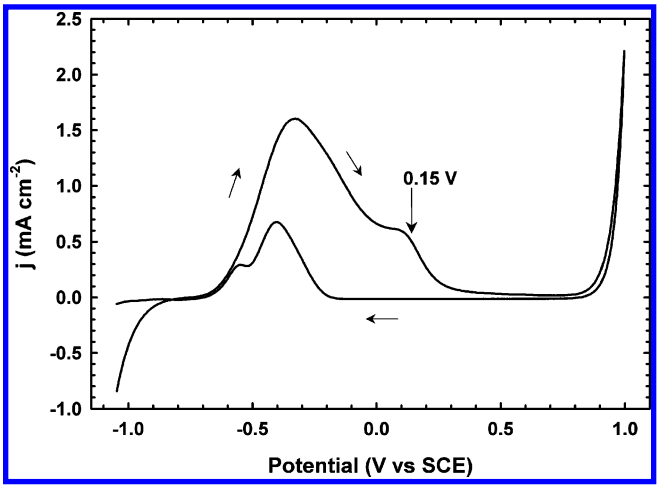

Figure 1. Voltammogram of the cobalt RDE in a deaerated 0.4 M $NaHCO_3$ solution at pH 8.9. $\omega = 1000$ rpm. $dE/dt = 0.005$ V s^{-1}.

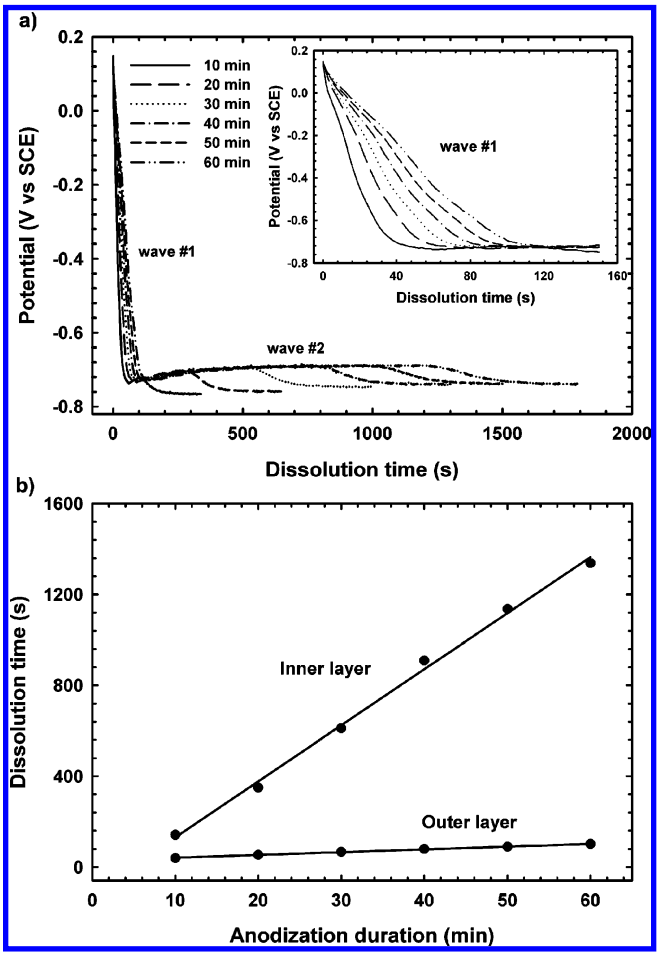

Figure 2. (a) Transient potential curves under open circuit conditions (inset: enlargement of wave #1), and (b) relationship between the dissolution time and the anodization duration for the inner and outer layers; in a 0.4 M $NaHCO_3$ deaerated solution for a cobalt RDE following anodization in the same medium at a potential of 0.15 V for 10 to 60 min. $\omega = 1000$ rpm.

papers have suggested the formation, in various aqueous environments, of sandwich-type cobalt oxide films constituted of an inner CoO layer and an outer Co_3O_4 layer.[9,17,22,24−32] However, this conclusion was mostly based on speculative arguments. Figure 2a shows the transient potential under open circuit conditions for a cobalt RDE obtained after an anodization at a potential of 0.15 V for a period of 10 to 60 min. Each

chronopotentiometric trace displays two waves which exhibit a fast dissolution step for the outer layer (wave #1; Figure 2a inset) and a slow dissolution step for the inner layer (wave #2). If it is assumed that both layers have similar solubility, it can be concluded that the outer layer is much thinner than the inner layer. When the electrode is removed from the solution just after the film formation, gently rinsed with deionized water, and dried prior to the open circuit potential (OCP) measurements, similar OCP curves are obtained. This observation demonstrates that the film composition is stable in air. It suggests that ex situ characterization of the films remains representative of the composition and structure of the film in the deaerated electrolytic medium. Figure 2b shows that the thickness of the inner layer increases approximately 20 times more rapidly than the thickness of the outer layer, which remains almost constant when the anodization duration increases. This result is consistent with a previous study concerning the cobalt oxidation in borate buffer,[22] which reports that the outer Co_3O_4 layer first grows until its thickness reaches a steady value. The initial growth of the outer layer is followed by a gradual increase of the inner CoO layer thickness. It is thus appropriate to propose that the inner layer growth is controlled by the diffusion of passivating species through the thin outer layer.

2. X-ray Photoelectron Spectroscopy. Figure 3a presents the Co 2p XP spectrum of the outer surface of the film grown for 45 min at 0.15 V. The Co $2p_{3/2}$ and Co $2p_{1/2}$ main peaks are located at 780.2 and 795.6 eV, respectively, while corresponding satellite peaks appear at 786.3 and 803.4 eV, respectively. Figures 3b and 3c display Co 2p XP spectra of standard Co_3O_4 and CoO, respectively. Higher Co 2p binding energies for standard CoO are attributed to a charging effect of the sample.[33] From the relative peak intensities of XP spectra presented in Figure 3, it is clear that the outer surface of the electrogenerated film is composed of Co_3O_4. Similar XP spectra for well-identified CoO and Co_3O_4 standards were reported in the literature.[34,35] As demonstrated in Figure 4, Ar^+ sputtering of standard Co_3O_4 leads to the formation of CoO. Therefore, XPS investigation of the underneath layer of electrogenerated films is not appropriate for the identification of the passive film inner layer.

3. Spectroscopic Ellipsometry. Spectroscopic ellipsometry (SE) is one of the most convenient, accurate, surface-sensitive, and nondestructive optical techniques to investigate the optical properties (complex refractive index, $N = n - ik$; n is the refractive index, k is the extinction coefficient), the microstructure, and the thickness of thin films.[36−40] Figure 5 presents the XP spectrum of cobalt substrate, recorded after polishing. The peak at 778.3 eV is assigned to Co $2p_{3/2}$ binding energy of bare cobalt,[41] while other peaks are characteristic of the XP signature of CoO (see Figure 3c). Since a stable native cobalt(II) oxide film (thickness < 10 nm) is formed on the polished cobalt following air exposition, the optical properties of the cobalt substrate were accurately determined using the Tauc−Lorentz 2 dispersion model[42] before performing the measurements on the films. Because the Tauc−Lorentz 2 dispersion model is commonly employed for dielectrics and semiconductors,[42] a good fit was obtained ($\chi^2 = 0.519$). After the optimization of the substrate dispersion model, a multiple but fast fitting procedure using the amorphous dispersion model was applied to a simple two-layer model, which consists of the cobalt substrate covered by a single overlayer. The amorphous dispersion model, developed by Forouhi and Bloomer,[43] is traditionally used for disordered or amorphous semiconductors and amorphous dielectrics.[39,43] Figure 6 shows an example of the

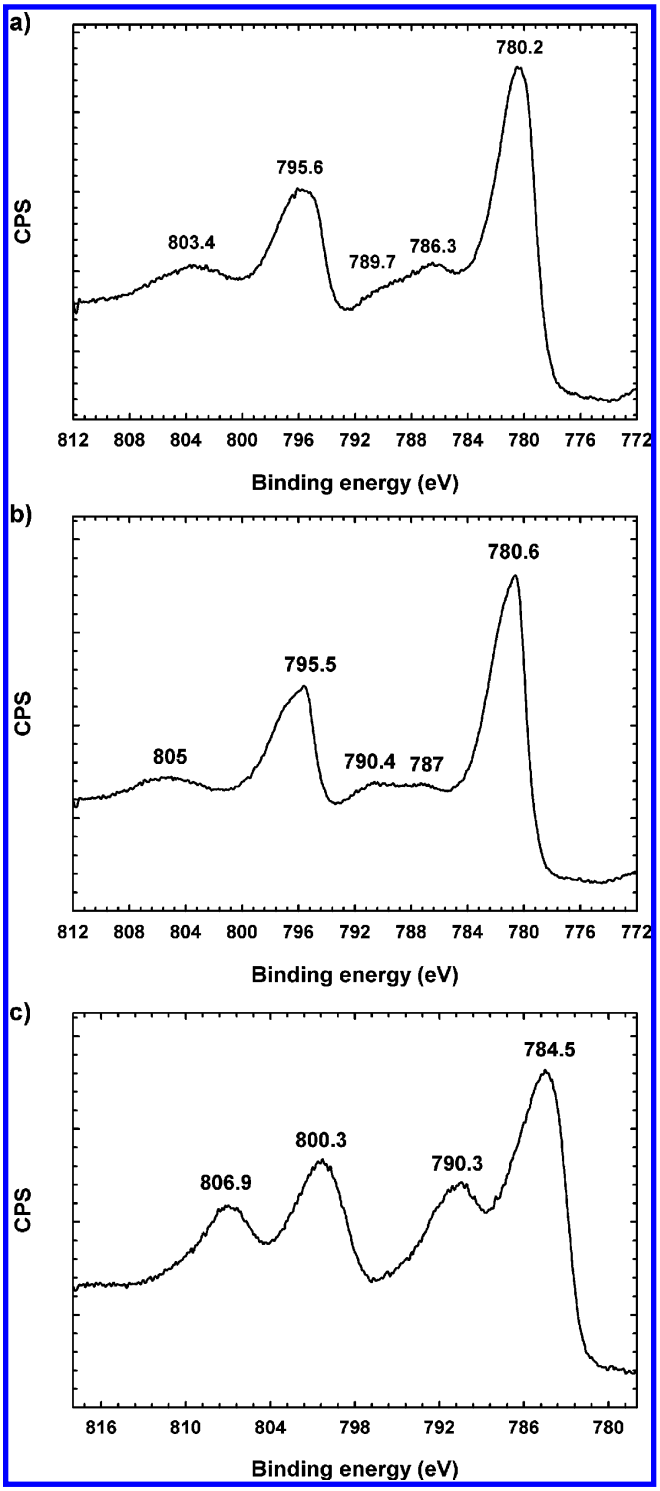

Figure 3. X-ray photoelectron Co 2p spectra of (a) the outer surface of the film grown for 45 min at 0.15 V, (b) standard Co_3O_4, and (c) standard CoO.

ellipsometric parameters *Is* ($\sin 2\psi \sin\Delta$) and *Ic* ($\sin 2\psi \cos\Delta$) as a function of λ, and the best fitting curves calculated using the amorphous dispersion model for the cobalt sample anodized for 35 min in the electrolytic medium. It must be pointed out that despite the complexity of the observed spectrum, an acceptable fit was nevertheless obtained ($\chi^2 = 27.7$).

3.1. Film Thickness Measurements. Figure 7 shows that the overall film thickness determined by SE increases linearly with the anodization duration, at a rate of 4.7 nm min^{-1}. Standard deviations (SD) on measurements were always less than 3%. To validate the film thicknesses determined by SE, two

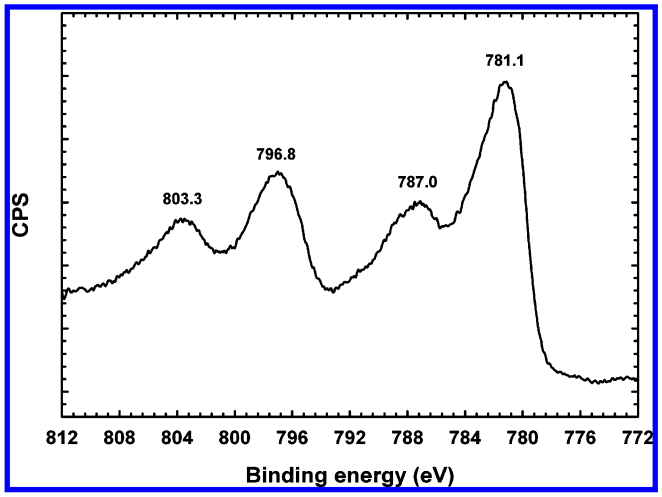

Figure 4. XP Co 2p spectrum of standard Co_3O_4 following sputtering with Ar^+ (1.5×10^{-6} Torr, 3 keV, 20 μA cm^{-2} for 20 min).

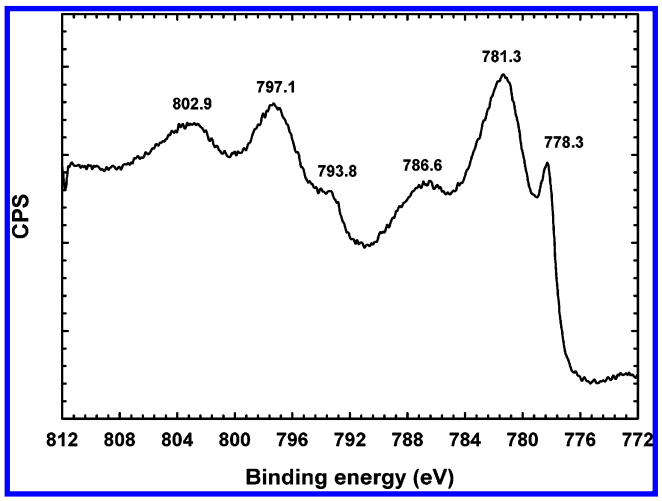

Figure 5. Cobalt 2p XP spectrum of the polished cobalt substrate.

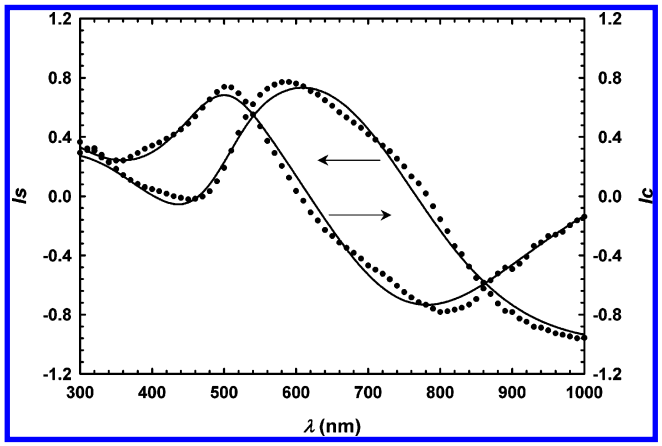

Figure 6. Ellipsometric parameters *Is* and *Ic* as a function of λ, and the best fitting curves calculated using the amorphous dispersion model (dotted line, experimental data; solid line, curve fit). Cobalt sample anodized for 35 min in a 0.4 M $NaHCO_3$ deaerated solution at pH 8.9. $\omega = 1000$ rpm.

mechanical methods were used: atomic force microscopy (AFM) and profilometry. AFM and profilometry measurements were performed following the creation of a step between the film and the substrate by the complete dissolution of a small section of the film using a drop of diluted HCl (see Figure 8). Such a procedure did not cause any dissolution of the substrate. The use of a step created by etching a part of the film using

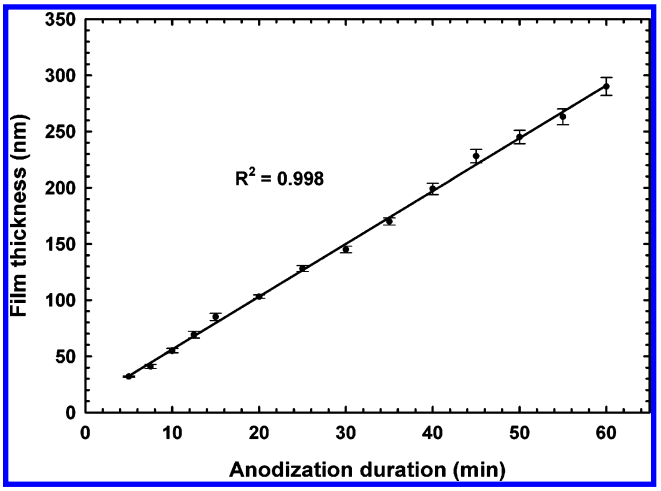

Figure 7. Film thickness, determined by spectroscopic ellipsometry, for a cobalt RDE anodized at a potential of 0.15 V for 5 to 60 min in a 0.4 M $NaHCO_3$ deaerated solution at pH 8.9. $\omega = 1000$ rpm.

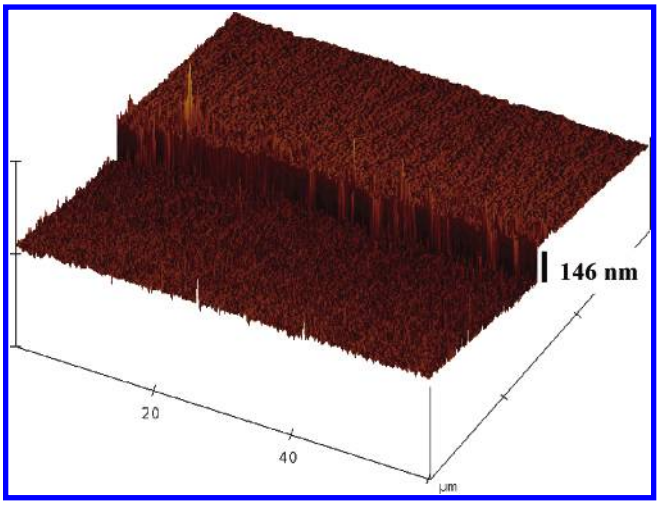

Figure 8. AFM image of the step formed by dissolution of an area of the film electrogenerated following the procedure described in the Experimental Details section.

HCl and H_2O_2 solution has already been reported for film thickness measurements of cobalt film sputtered on a silicon substrate.[44] Table 1 shows that even though the MSE on SE results are sometimes high, the results obtained from SE measurements are in very good agreement with AFM and profilometry results. High MSE values are acceptable as long as SE results are confirmed using other techniques.[46]

Our results show that among the three methods used for film characterization (SE, AFM, and profilometry), SE is the most accurate, simplest, and fastest method for thickness determination of such films since it provides the lowest SD on thickness measurements. Moreover, SE is the only technique allowing the thickness determination of the thinnest films. The good agreement between results obtained by SE with mechanical techniques further supports the reliability of the amorphous dispersion model.

3.2. Optical Parameters: Complex Refractive Index, $N = n - ik$. Figure 9a presents a typical dispersion of the real part of the complex refractive index (n) as a function of the wavelength (λ) obtained by SE, while Figure 9b shows the variation of n at 632.8 nm for the electrogenerated films as a function of the anodization duration. Since ellipsometric measurements are traditionally performed using monochromatic incidence light of wavelength 632.8 nm,[23,38,43,44,47−53] the optical parameters

TABLE 1: Film Thicknesses Determined by Ellipsometry, Atomic Force Microscopy, and Profilometry, as a Function of the Anodization Duration[a]

	ellipsometry			atomic force microscopy		profilometry	
anodization duration (min)	thickness (nm)	SD[b] (nm)	MSE [c]	thickness (nm)	SD (nm) ($n = 12$)	thickness (nm)	SD (nm) ($n = 5$)
5	31	1	0.6				
7.5	42	2	5.1				
10	55	2	7.7				
12.5	69	3	24.2				
15	85	3	31.9			80	11
20	103	2	16.0	105	8	102	14
25	128	3	22.4	124	6	131	5
30	146	3	26.5	146	5	154	13
35	170	3	27.7	168	6	178	6
40	199	5	39.7	196	8	208	5
45	229	6	44.4	219	7	228	7
50	245	6	46.8	230	16	251	3
55	263	7	52.6	244	13	255	10
60	290	8	71.2	279	16	283	9

[a] Films were electrogenerated following the procedure described in the Experimental Details section. [b] Errors on measurements which are calculated during the Marquardt minimization process. [c] The measured ellipsometric spectra are fitted by minimizing the squared difference (χ^2 or MSE) between the measured and calculated values of the ellipsometric parameters (*Is* and *Ic*) given by $\mathrm{MSE} = \chi^2 = [1/(2N - P)]\sum_i^N[(I_{s,i}^{\mathrm{exp}} - I_{s,i}^{\mathrm{cal}})^2 + (I_{c,i}^{\mathrm{exp}} - I_{c,i}^{\mathrm{cal}})^2]$, where N is the number of data points and P is the number of model parameters.[45]

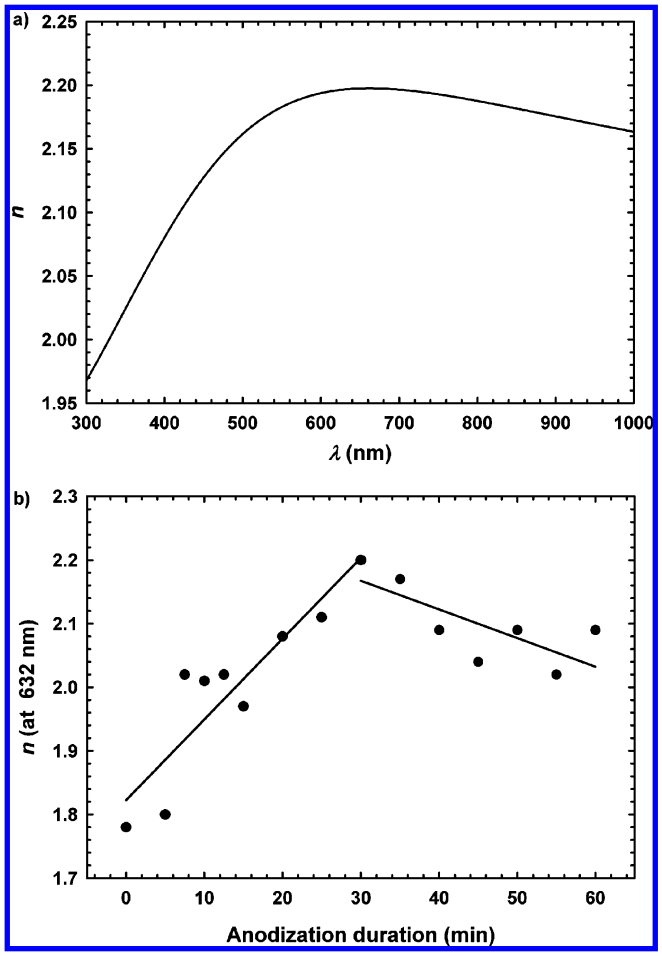

Figure 9. (a) Variation of the real part of the refractive index (n) as a function of the wavelength (λ), and (b) variation of n at a wavelength 632.8 nm as a function of the anodization duration; for a cobalt RDE anodized at a potential of 0.15 V in a 0.4 M $NaHCO_3$ deaerated solution at pH 8.9. $\omega = 1000$ rpm. (30-minute anodization for a)).

determined in the present study are reported at this wavelength. It can be seen that the refractive index of the electrode surface increases from 1.78 (cobalt substrate) to 2.20 during the first 30 min, while it decreases from 2.20 to 2.09 in the 30- to 60-minute range ($\bar{n} = 2.05 \pm 0.09$). These data demonstrate that the compactness of the film increases during the first 30 min, while the film becomes less densely packed during the last 30 min.[2,47,54−58] Previous studies have shown smaller refractive index values for samples of thicknesses greater than 100 nm, due to the lower rigidity and greater porosity of the samples.[59] The diminution of the refractive index can also be interpreted in terms of higher hydration of the film.[48] The values obtained for the refractive indices are close to those reported in the literature for CoO (2.4 ± 0.2).[32,50,60,61] Variations of the refractive index for CoO reported in the literature can be explained by the preparation method of the films.[54] The refractive index of Co_3O_4 is generally higher (3.2).[22,32] For comparison, refractive indices for iron oxides reported in the literature vary from 2.2 to 3.0.[53] Finally, the average value (0.18 ± 0.03; $n = 14$) of the imaginary part of the complex refractive index (k) for the films electrogenerated from 5 to 60 min is close to values reported in the literature for CoO that range from 0.1 to 0.4.[22,32,60] Therefore, the complex refractive indices determined for the films electrogenerated on cobalt suggest that the film is mainly composed of CoO. Because strong absorption is accompanied by high reflectivity,[62] it explains that k values determined by SE for bare cobalt (dispersed from ~2 to 6) are higher than those for the films (dispersed from ~0.01 to 0.36) for the whole range of wavelengths investigated (i.e., 300−1000 nm).

4. Physical Aspects of Anodized Cobalt Surfaces. Figure 10a shows the different bright colors generated by various thicknesses of films obtained by potentiostatic polarization at 0.15 V of a cobalt RDE. Their uniform colors, as well as their interesting resistance to localized corrosion,[9] lead us to believe that these films are well structured. SEM images presented in Figures 11a and 11b show the complete and uniform coverage of the bare cobalt electrode obtained by anodization of the electrode at a potential of 0.15 V for 45 min. As seen in Figure 10b, 30 min polarization at a potential of 0.1 V, located at the maximum of the second anodic dissolution peak, leads to the formation of a nonuniformly colored film. This is explained by the parallel dissolution and passivation of the electrode surface. Indeed, the thickness of the growing film is not regular, varying from 169 nm in the center to 267 nm on the outside of the electrode. Moreover, the SEM image of this surface clearly exhibits important film defects existing on the anodized substrate

Figure 10. Photograph of the films electrogenerated on a cobalt RDE anodized at a potential of (a) 0.15 V and (b) 0.1 and 0.2 V; in a 0.4 M $NaHCO_3$ deaerated solution at pH 8.9. $\omega = 1000$ rpm. For (b), 30 min anodization.

(Figure 11c). On the other hand, polarization at a potential of 0.2 V leads to the electrogeneration of a brown-colored film, independently of the polarization duration. Its low thickness, i.e., 41 nm, obtained from a polarization duration of 30 min, is attributed to the low current density and consequently to a weaker anodization charge. It is seen in an SEM image of this surface (Figure 11d) that the film is so thin that substrate defects are visible.

5. Specular Reflectance UV−Vis−NIR Spectrophotometry. Figure 12 shows an example of a specular reflectance UV−vis−NIR spectrum recorded in the wavelength range of 400 to 1500 nm for the bluish green color film electrogenerated for 45 min. The spectrum displays a maximum reflectance in the visible region at $\lambda = 502$ nm. Table 2 presents the wavelengths at which some other electrogenerated films exhibit maximum constructive interference of the UV−vis−NIR light under specular reflectance conditions, as a function of the anodization duration. Such results confirm the transparent character of the films, as well as the occurrence of iridescence. This interference phenomenon, defined as constructive light interference between the beam reflected at the outer film−air interface and the inner metal−film interface,[63,64] induces the coloration of the films because their thicknesses, as determined by SE, AFM, and profilometry, are in the order of the wavelength of visible light.[65,66] It has already been mainly observed for titanium (e.g., refs 46, 63, 64, 67−70) and stainless steel (e.g., refs 71−73), but is here reported for the first time for cobalt. The aim of this section is then to demonstrate that wavelengths constructively reinforced by interference from the electrogenerated thin films can be used to accurately calculate film thicknesses and, consequently, to confirm the values of the refractive indices determined by SE. The optical system analyzed by UV−vis−NIR spectrophotometry in the present study is composed of a dielectric medium (i.e., air), a semiconducting material (i.e., ceramic-type film, from ref 7 and model fitted by SE), and a conducting substrate (i.e., metallic cobalt). To determine the exact interference conditions, phase changes upon reflection at both interfaces (air/film and film/substrate) of the system must be considered. Since the position of the C 1s peak on the XP spectra of electrogenerated films (284.8 eV; figures not shown) shows the conducting or semiconducting character of the films,[33] a phase change rather complicated than 0 or π is expected.[74−77] For the considered interfaces, the following relationship has been proposed for the determination of the phase change upon reflection:[75]

$$\phi(\lambda) = \arctan\left[\frac{2k(\lambda)}{1 - k^2(\lambda) - n^2(\lambda)}\right] \qquad (1)$$

where $\phi(\lambda)$ is the phase change as a function of light wavelength, $k(\lambda)$ and $n(\lambda)$ are the extinction coefficient and refractive index, respectively, of the material on which light is reflected and dephased.[62,75] The additional phase change $\phi(\lambda)$ are sometimes neglected.[77] It is important to notice that neglecting phase changes upon reflection at both interfaces leads, in the present case, to overestimation of film thicknesses by 5 to 15% compared with those determined by SE, AFM, and profilometry. Surprisingly, no consensus has been reached in the literature regarding the sign and amplitude of phase change at the dielectric/metal interface.[76] In the present study, by using eq 1 to evaluate phase change upon near normal reflection, it was found that thicknesses determined from UV−vis−NIR experiments using unpolarized incident light beam, closely correspond to those determined from SE experiments. Figure 13 presents typical optical phase changes at air/film ($\phi(\lambda)_{\text{air/film}}$) and film/substrate ($\phi(\lambda)_{\text{film/substrate}}$) interfaces calculated using eq 1 for the film electrogenerated by 30 min anodization at 0.15 V. From these results, the difference in optical path length between interfering rays is given by the relationship[77]

$$\Lambda = 2nd\cos\theta_r + \phi(\lambda)_{\text{air/film}} + \phi(\lambda)_{\text{film/substrate}} \qquad (2)$$

where n is the refractive index of the film, d is the film thickness, m is the interference order, and θ_r is the angle of incidence of light beam reflected at the film/substrate interface.[66,67,77] This relationship allows to consider the optical retardation due to the geometry and density of the film (thickness and refractive index), as well as the retardation due to reflection at both interfaces. Constructive interference occurs when $\Lambda = m\lambda$, where λ is the wavelength of maximum reflectance.[66,67] Considering the reinforced wavelengths in the visible light region ($m = 2$) reported in Table 2 and the refractive index determined by SE of the material at $\lambda_{\text{reinforced}}$, the film thicknesses have been calculated and are reported in Table 3. It is seen that these results are in very good agreement with those reported in Table 1, confirming the exactness of the refractive indices of films determined by SE at the considered wavelengths. Since the Tauc−Lorentz 2 dispersion model does not reasonably fit experimental data in the UV region ($\lambda < 270$ nm), the thickness determination of films generated during 5 to 35 min anodization cannot be evaluated using UV−vis−NIR spectrophotometry.

6. Raman Spectroscopy. At this point, OCP and XPS experiments have clearly demonstrated that the films electrogenerated as described above are constituted of a Co_3O_4 thin outer layer, while SE experiments suggest that the films are mainly composed of amorphous CoO. To confirm the main chemical composition of the films, we have used Raman spectroscopy. The Co_3O_4 oxide should crystallize in the normal spinel structure with Co^{2+} and Co^{3+} located at tetrahedral and octahedral sites, respectively.[78] For this structure, the A_{1g}, E_g, and three T_{2g} modes are Raman active.[79−82] Concerning the CoO oxide, it is well known that, at room temperature, its crystal structure is of face-centered cubic (fcc) type, in which Co^{2+} ions are octahedrally coordinated to six O^{2-} ions.[5,83−85] Then, theoretically, the O_h symmetry of CoO should lead to the observation of at least three Raman active modes (A_{1g}, E_g, and T_{2g}).[86] However, despite this well-accepted theory, very different

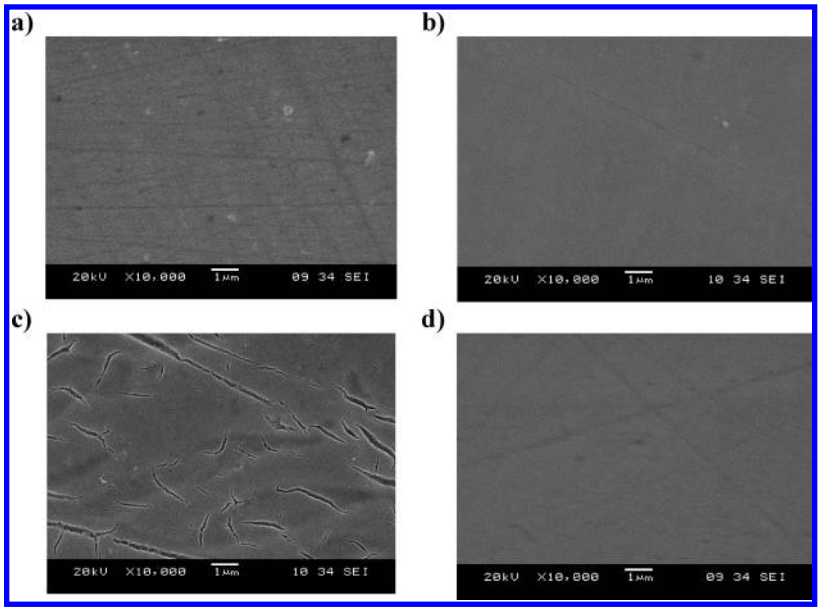

Figure 11. SEM images of (a) bare cobalt electrode; cobalt RDE (ω = 1000 rpm) anodized in a 0.4 M $NaHCO_3$ deaerated solution at pH 8.9, at a potential of (b) 0.15 V for 45 min, (c) 0.1 V for 30 min, (d) 0.2 V for 30 min.

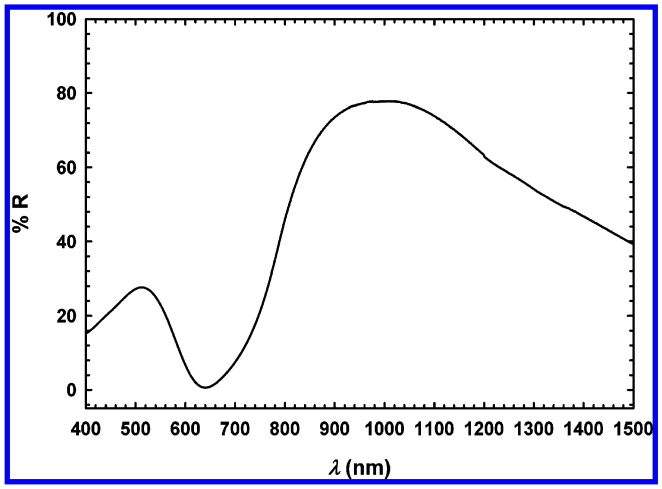

Figure 12. Specular reflectance UV−vis−NIR spectrum for a cobalt RDE anodized during 45 min at 0.15 V in a 0.4 M $NaHCO_3$ deaerated solution at pH 8.9. ω = 1000 rpm.

TABLE 2: Constructive Interference Maxima as a Function of Anodization Duration (40 to 60 min) for the Films Electrogenerated Following the Procedure Described in the Experimental Details Section[a]

anodization duration (min)	$\lambda_{reinforced}$ (nm) (for $m = 2$)
40	453
45	502
50	550
55	562
60	600

[a] Spectra were obtained under specular reflection conditions, in the wavelength range of 400 to 1500 nm.

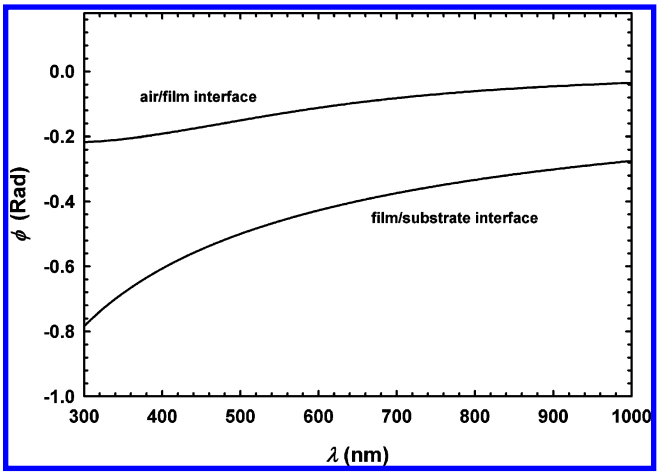

Figure 13. Typical optical phase changes at air/film ($\phi(\lambda)_{air/film}$) and film/substrate ($\phi(\lambda)_{film/substrate}$) interfaces calculated using eq 1 for films electrogenerated by anodization at 0.15 V (sample anodized 30 min).

TABLE 3: Film Thicknesses Determined from UV−Vis−NIR Interference Conditions[a]

anodization duration (min)	film thickness (nm)
40	206
45	231
50	247
55	261
60	273

[a] Films were electrogenerated following the procedure described in the Experimental Details section.

Raman spectra of CoO with 2 to 5 bands have been reported in the literature.[9,49,87−90] Moreover, the ambiguity in the assignment of the Raman bands of CoO has recently been reported.[91] Similarly, the interpretation of Raman spectra of the well-known compound wüstite (FeO) is still unclear.[92−95] Interestingly, Thibeau et al.[94] and de Faria et al.[92] reported that the laser beam used for excitation can convert FeO to Fe_3O_4. Moreover, an increasing temperature is known to cause a red-shift of the Raman active vibrations for different oxides.[92,96−99] Hence, in the present work, the influence of the excitation laser intensity has been investigated on an electrogenerated cobalt oxide film. Figure 14a presents a Raman spectrum of the film electrogenerated during 35 min and recorded using a 4 μW excitation laser intensity. It shows two main peaks, located at 484 and 693 cm^{-1}, which correspond to the Raman active modes E_g and A_{1g}, respectively.[79−82,86,92] A broad band located between 500 and 650 cm^{-1} is assigned to anharmonic interactions in the film structure.[92] Since amorphous solids usually give broader Raman

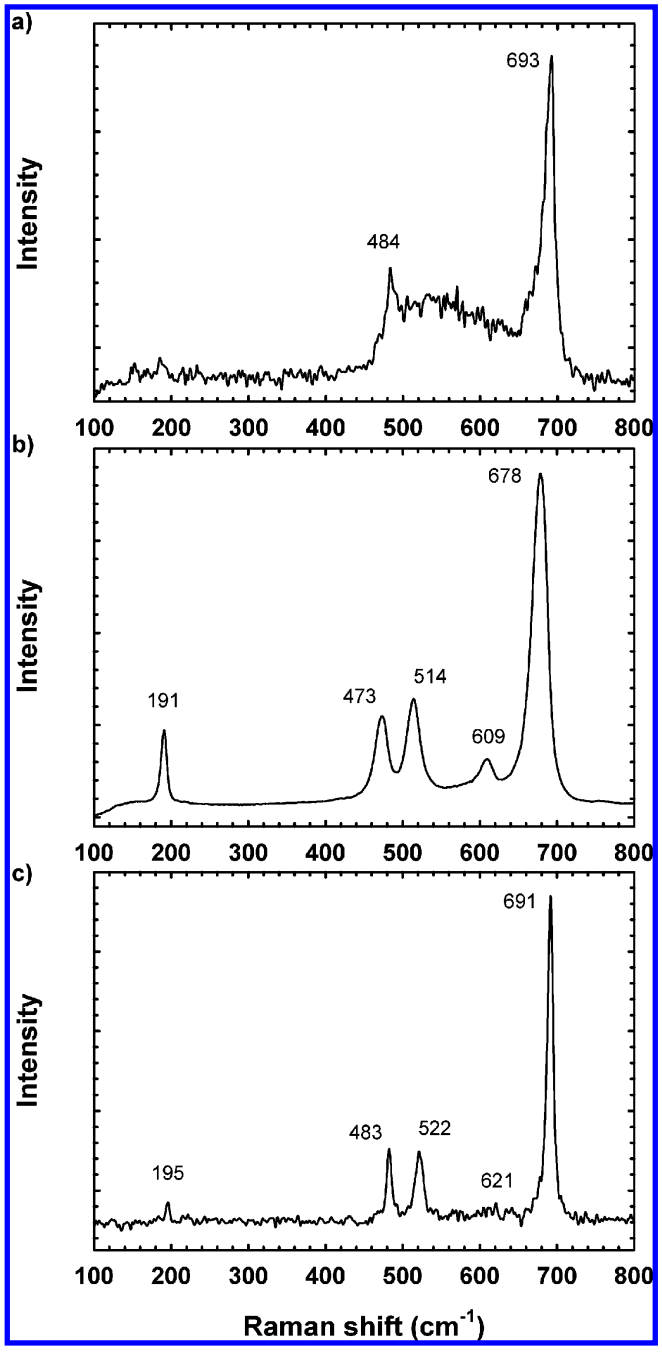

Figure 14. Raman spectra of the film electrogenerated for 35 min following the procedure described in the Experimental Details section. Spectra were recorded on the same spot of the film, using successively excitation laser intensities of (a) 4 μW; (b) 4 mW; and (c) 4 μW.

bands than crystalline solids,[100] it is concluded that the electrogenerated films possess an amorphous character. This result is supported by the fact that only the amorphous dispersion model has given correlatable results in SE and that all XRD experiments performed (multiple incidence angle and grazing incidence angle) suggest an amorphous character for the films since no diffraction peaks were observed (figures not shown). Moreover, since the Raman spectrum of the CoO standard presented in Figure 15a, also recorded using the 4 μW excitation laser, is quite similar to the Raman spectrum shown in Figure 14a, it can be concluded that the film electrogenerated on the cobalt disk is mainly composed of amorphous CoO. The spectrum presented in Figure 14b was recorded on the same spot of the film as the spectrum presented in Figure 14a, except

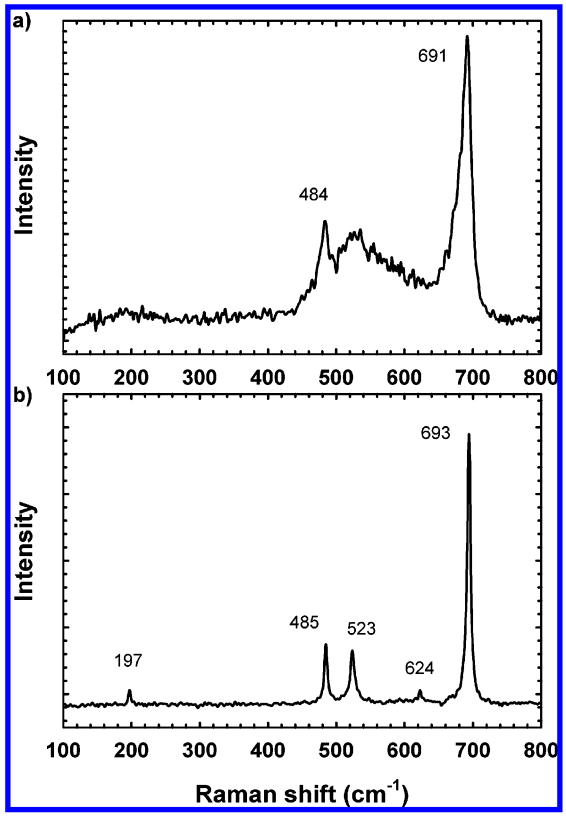

Figure 15. Raman spectra of standard (a) CoO and (b) Co_3O_4; using excitation laser beam intensity of 4 μW.

that the laser intensity was increased to 4 mW. This spectrum clearly exhibits five well-defined Raman peaks at 191, 514, 609, 473, and 678 cm^{-1}, assigned to the Raman active modes of Co_3O_4, i.e., T_{2g}, E_g, and A_{1g} symmetries, respectively.[78] Furthermore, the effect of temperature is clearly evidenced since Raman bands initially located at 693 and 484 cm^{-1} (Figure 14a) are red-shifted to 678 and 473 cm^{-1}, respectively. Figure 14c presents the third Raman spectrum recorded on the same spot of the film, using for a second time the 4 μW laser intensity. However, this Raman spectrum exhibits important differences from the first Raman spectrum recorded with the same 4 μW excitation laser (Figure 14a). Indeed, on the spectrum of Figure 14c, five bands are distinguished at 195, 483, 522, 621, and 691 cm^{-1}. These bands are present on the Raman spectrum of Co_3O_4 standard recorded using 4 μW excitation laser (Figure 15b). This observation demonstrates that the 4 mW laser intensity causes a conversion of the nature of the electrogenerated film, which is also true for films formed by other anodization durations. Indeed, the electrogenerated CoO film is oxidized to Co_3O_4 when it is exposed to higher laser intensity. The importance of using very low laser beam intensity to avoid local overheating of the analyte that causes red-shift of the bands as well as modification of the nature of the film is thus clearly demonstrated. To the best of our knowledge, no Raman spectra of oxides have been recorded using laser intensity as low as a few μW. This can be explained by the fact that Raman spectroscopy is intrinsically a weak effect and because oxide films are often thin, making it difficult to obtain good quality Raman spectra. Because of its inherent thickness, the outer Co_3O_4 layer, present on the outer surface of the electrogenerated films, was not observed by Raman spectroscopy. However, its existence has been previously suggested from galvanostatic reduction[9] and OCP experiments, and confirmed by XPS experiments.

Conclusion

A novel electrochemical procedure performed in a mild aqueous bicarbonate media was applied to generate new amorphous cobalt oxide films brightly and uniformly colored by iridescence, and having a highly protective character against localized corrosion induced by chloride ions. The optical and physical properties of these films were extensively investigated using various mechanical and spectroscopic techniques. Spectroscopic ellipsometry, using the amorphous dispersion model, was used to evaluate the film thickness (ranged from 31 to 290 nm) and the complex refractive index ($N = 2.05 + i0.18$, at 632.8 nm) of the electrogenerated films. Film thicknesses were also determined using atomic force microscopy and profilometry. The relationship between film thickness and constructive interference wavelengths obtained from UV−vis−NIR spectrophotometry confirms the values of refractive index (n) previously estimated by spectroscopic ellipsometry. Since we have found that a high laser intensity modifies the nature of the oxide film, Raman spectroscopy was performed, for the first time, using a laser line intensity of 4 μW to demonstrate that the film is essentially composed of amorphous CoO. Finally, XPS and OCP measurements have successfully demonstrated the presence of a thin Co_3O_4 layer on the CoO surface.

Acknowledgment. This work was supported by a scholarship and a discovery grant from the Natural Sciences and Engineering Research Council of Canada (NSERC).

References and Notes

(1) Chidambaram, K.; Malhotra, L. K.; Chopra, K. L. *Thin Solid Films* **1982**, *87*, 365.
(2) Eze, F. C. *J. Phys. D: Appl. Phys.* **1999**, *32*, 533.
(3) Patil, P. S.; Kadam, L. D.; Lokhande, C. D. *Thin Solid Films* **1996**, *272*, 29.
(4) Brundle, C. R.; Chuang, T. J.; Rice, D. W. *Surf. Sci.* **1976**, *60*, 286.
(5) Hagelin-Weaver, H. A. E.; Hoflund, G. B.; Minahan, D. M.; Salaita, G. N. *Appl. Surf. Sci.* **2004**, *235*, 420.
(6) Patil, P. S.; Kadam, L. D.; Lokhande, C. D. *Sol. Energ. Mater. Sol. C.* **1998**, *53*, 229.
(7) Barreca, D.; Massignan, C.; Daolio, S.; Fabrizio, M.; Piccirillo, C.; Armelao, L.; Tondello, E. *Chem. Mater.* **2001**, *13*, 588.
(8) Gulino, A.; Dapporto, P.; Rossi, P.; Fragalà, I. *Chem. Mater.* **2003**, *15*, 3748.
(9) Gallant, D.; Simard, S. *Corros. Sci.* **2005**, *47*, 1810.
(10) Nuse, J. D.; Falkowski, J. A. *Proceedings of the Aerospace/Airline Plating and Metal Finishing Forum in Cincinnati*; Cincinnati, OH, 2000.
(11) Kadam, L. D.; Pawar, S. H.; Patil, P. S. *Mater. Chem. Phys.* **2001**, *68*, 280.
(12) Monk, P. M. S.; Chester, S. L.; Higham, D. S.; Partridge, R. D. *Electrochim. Acta* **1994**, *39*, 2277.
(13) Švegl, F.; Orel, B.; Hutchins, M. G.; Kalcher, K. *J. Electrochem. Soc.* **1996**, *143*, 1532.
(14) Maruyama, T.; Arai, S. *J. Electrochem. Soc.* **1996**, *143*, 1383.
(15) Seike, T.; Nagai, J. *Sol. Energ. Mater.* **1991**, *22*, 107.
(16) Polo da Fonseca, C. N.; De Paoli, M.-A.; Gorenstein, A. *Sol. Energ. Mater. Sol. C* **1994**, *33*, 73.
(17) Burke, L. D.; Murphy, O. J. *J. Electroanal. Chem.* **1980**, *109*, 373.
(18) Burke, L. D.; Lyons, M. E.; Murphy, O. J. *J. Electroanal. Chem.* **1982**, *132*, 247.
(19) Davies, D. H.; Burstein, G. T. *Corros. Sci.* **1980**, *20*, 973.
(20) Gervasi, C. A.; Biaggio, S. R.; Vilche, J. R.; Arvia, A. J. *Corros. Sci.* **1989**, *29*, 427.
(21) Gallant, D.; Pézolet, M.; Jacques, A.; Simard, S. *Corros. Sci.*, in press.
(22) Ohtsuka, T.; Sato, N. *J. Electrochem. Soc.* **1981**, *128*, 2522.
(23) Paik, W.-K.; Koh, S. *Bull. Korean Chem. Soc.* **1991**, *12*, 540.
(24) Sato, N.; Ohtsuka, T. *J. Electrochem. Soc.* **1978**, *125*, 1735.
(25) Gervasi, C. A. *J. Braz. Chem. Soc.* **1997**, *8*, 169.
(26) Ohtsuka, T.; Kudo, K.; Sato, N. *J. Jpn. Inst. Met.* **1976**, *40*, 124.
(27) Burstein, G. T.; Davies, D. H. *Corros. Sci.* **1980**, *20*, 989.
(28) Gomez Meier, H.; Vilche, J. R.; Arvia, A. J. *J. Electroanal. Chem.* **1982**, *138*, 367.
(29) Gervasi, C. A.; Biaggio, S. R.; Vilche, J. R.; Arvia, A. J. *Electrochim. Acta* **1991**, *36*, 2147.
(30) Gervasi, C. A.; Vilche, J. R.; Alvarez, P. E. *Electrochim. Acta* **1996**, *41*, 455.
(31) Gervasi, C. A.; Varela, F. E.; Vilche, J. R. *Mater. Sci. Forum* **1998**, *289−292*, 1057.
(32) Ohtsuka, T.; Sato, N. *J. Electroanal. Chem.* **1983**, *147*, 167.
(33) Palchan, I.; Crespin, M.; Estrade-Szwarckopf, H.; Rousseau, B. *Chem. Phys. Lett.* **1989**, *157*, 321.
(34) Carson, G. A.; Nassir, M. H.; Langell, M. A. *J. Vac. Sci. Technol. A* **1996**, *14*, 1637.
(35) Petitto, S. C.; Langell, M. A. *J. Vac. Sci. Technol. A* **2004**, *22*, 1690.
(36) Girardeau, T.; Camelio, S.; Traverse, A.; Lignou, F.; Allain, J.; Naudon, A.; Guérin, Ph. *J. Appl. Phys.* **2001**, *90*, 1788.
(37) Urban, F. K.; Hosseini-Tehrani, A.; Khabari, A.; Griffiths, P.; Bungay, C.; Petrov, I.; Kim, Y. *Thin Solid Films* **2002**, *408*, 211.
(38) Chen, Q.; Gu, D.; Gan, F. *Physica B* **1995**, *212*, 189.
(39) Gupta, S.; Weiner, B. R.; Morell, G. *J. Appl. Phys.* **2002**, *92*, 5457.
(40) Hristova, E.; Arsov, Lj.; Popov, B. N.; White, R. E. *J. Electrochem. Soc.* **1997**, *144*, 2318.
(41) Mandale, A. B.; Badrinarayanan, S.; Date, S. K.; Sinha, A. P. B. *J. Electron Spectrosc. Relat. Phenom.* **1984**, *33*, 61.
(42) Jellison, G. E., Jr.; Modine, F. A. *Appl. Phys. Lett.* **1996**, *69*, 371.
(43) Forouhi, A. R.; Bloomer, I. *Phys. Rev. B* **1986**, *34*, 7018.
(44) Ko, S.-H.; Murarka, S. P.; Sitaram, A. R. *J. Appl. Phys.* **1992**, *71*, 5892.
(45) Bhattacharyya, D.; Biswas, A.; Sahoo, N. K. *Appl. Surf. Sci.* **2004**, *233*, 155.
(46) Van Gils, S.; Mast, P.; Stijns, E.; Terryn, H. *Surf. Coat. Technol.* **2004**, *185*, 303.
(47) Riley, D. W.; Gerhardt, R. A. *J. Appl. Phys.* **2000**, *87*, 2169.
(48) Ohtsuka, T.; Otsuki, T. *Corros. Sci.* **2003**, *45*, 1793.
(49) Nan, J.; Yang, Y.; Lin, Z. *Electrochim. Acta* **2001**, *46*, 1767.
(50) Görts, P. C.; Vredenberg, A. M.; Habraken, F. H. P. M. *Surf. Sci.* **1997**, *370*, L207.
(51) Dell'Oca, C. J.; Fleming, P. J. *J. Electrochem. Soc.* **1976**, *123*, 1487.
(52) Kuo, D.-H.; Tzeng, K.-H. *Thin Solid Films* **2004**, *460*, 327.
(53) Graat, P. C. J.; Somers, M. A. J.; Mittemeijer, E. J. *Thin Solid Films* **1999**, *340*, 87.
(54) Ando, M.; Kadono, K.; Kamada, K.; Ohta, K. *Thin Solid Films* **2004**, *446*, 271.
(55) Hernández Ubeda, M.; Herrera, H.; Mishima, H. T.; López de Mishima, B. A.; Villullas, H. M.; López Teijelo, M. *Electrochim. Acta* **1998**, *44*, 513.
(56) Barrera, E.; Viveros, T.; Avila, A.; Quintana, P.; Morales, M.; Batina, N. *Thin Solid Films* **1999**, *346*, 138.
(57) Geotti-Bianchini, F.; Guglielmi, M.; Polato, P.; Soraru, G. D. *J. Non-Cryst. Solids* **1984**, *63*, 251.
(58) Schnyder, B.; Kötz, R. *J. Electroanal. Chem.* **1992**, *339*, 167.
(59) Cruz, C. M. G. S.; Ticianelli, E. A. *J. Electroanal. Chem.* **1997**, *428*, 185.
(60) Paik, W.-K.; Bockris, J. O'M. *Surf. Sci.* **1971**, *28*, 61.
(61) Powell, R. J.; Spicer, W. E. *Phys. Rev. B* **1970**, *2*, 2182.
(62) Born, M.; Wolf, E. *Principles of Optics*; Pergamon: New York, 1980.
(63) Hrapovic, S.; Luan, B. L.; D'Amours, M.; Vatankhah, G.; Jerkiewicz, G. *Langmuir*, **2001**, *17*, 3051.
(64) Jerkiewicz, G.; Strzelecki, H.; Wieckowski, A. *Langmuir* **1996**, *12*, 1005.
(65) Nassau, K. *The Physics and Chemistry of Color*; Wiley: New York, 2001.
(66) Pfaff, G.; Reynders, P. *Chem. Rev.* **1999**, *99*, 1963.
(67) Delplancke, J.-L.; Degrez, M.; Fontana, A.; Winand, R. *Surf. Technol.* **1982**, *16*, 153.
(68) Piontelli, R.; Pedeferri, P. *J. Electrochem. Soc.* **1968**, *115*, 1046.
(69) Gaul, E. *J. Chem. Educ.* **1993**, *70*, 176.
(70) Huang, C.-C.; Tang, J.-c.; Tao, W.-H. *Sol. Energ. Mater. Sol. C* **2004**, *83*, 15.
(71) Conrrado, R.; Bocchi, N.; Rocha-Filho, R. C.; Biaggio, S. R. *Electrochim. Acta* **2003**, *48*, 2417.
(72) Fujimoto, S.; Tsujino, K.; Shibata, T. *Electrochim. Acta* **2001**, *47*, 543.
(73) Ogura, K.; Sakurai, K.; Uehara, S. *J. Electrochem. Soc.* **1994**, *141*, 648.
(74) Tan, C. Z. *Physica B* **1999**, *262*, 98.
(75) Harasaki, A.; Schmit, J.; Wyant, J. C. *Appl. Optics* **2001**, *40*, 2102.
(76) Briscoe, W. H.; Horn, R. G. *J. Opt. A: Pure Appl. Opt.* **2004**, *6*, 112.
(77) Hecht, E. *Optics*; Addison-Wesley: San Francisco, 2002.
(78) Hadjiev, V. G.; Iliev, M. N.; Vergilov, I. V. *J. Phys. C: Solid State Phys.* **1988**, *21*, L199.

(79) O'Horo, M. P.; Frisillo, A. L.; White, W. B. *J. Phys. Chem. Solids* **1973**, *34*, 23.
(80) de Wijs, G. A.; Fang, C. M.; Kresse, G.; de With, G. *Phys. Rev. B* **2002**, *65*, 094305-1.
(81) Shebanova, O. N.; Lazor, P. *J. Solid State Chem.* **2003**, *174*, 424.
(82) Shebanova, O. N.; Lazor, P. *J. Chem. Phys.* **2003**, *119*, 6100.
(83) Guo, Q.; Mao, H.-K.; Hu, J.; Shu, J.; Hemley, R. J. *J. Phys.: Condens. Matter* **2002**, *14*, 11369.
(84) Larramona, G.; Gutiérrez, C. *J. Electroanal. Chem.* **1990**, *293*, 237.
(85) Gielisse, P. J.; Plendi, J. N.; Mansur, L. C.; Marshall, R.; Mitra, S. S.; Mykolajewycz, R.; Smakula, A. *J. Appl. Phys.* **1965**, *36*, 2446.
(86) Nakamoto, K. *Infrared and Raman Spectra of Inorganic and Coordination Compounds Part A: Theory and Applications in Inorganic Chemistry*; Wiley: New York, 1997.
(87) Vuurman, M. A.; Stufkens, D. J.; Oskam, A.; Deo, G.; Wachs, I. E. *J. Chem. Soc., Faraday Trans.* **1996**, *92*, 3259.
(88) Choi, H. C.; Jung, Y. M.; Noda, I.; Kim, S. B. *J. Phys. Chem. B* **2003**, *107*, 5806.
(89) Calderón, J. A.; Mattos, O. R.; Barcia, O. E.; Córdoba de Torresi, S. I.; Pereira da Silva, J. E. *Electrochim. Acta* **2002**, *47*, 4531.
(90) Melendres, C. A.; Xu, S. *J. Electrochem. Soc.* **1984**, *131*, 2239.
(91) Llorca, J.; de la Piscina, P. R.; Dalmon, J.-A.; Homs, N. *Chem. Mater.* **2004**, *16*, 3573.
(92) de Faria, D. L. A.; Venâncio Silva, S.; de Oliveira, M. T. *J. Raman Spectrosc.* **1997**, *28*, 873.
(93) Singh Raman, R. K.; Gleeson, B.; Young, D. J. *Mater. Sci. Technol. Ser.* **1998**, *14*, 373.
(94) Thibeau, R. J.; Brown, C. W.; Heidersbach, R. H. *Appl. Spectrosc.* **1978**, *32*, 532.
(95) England, W. A.; Bennett, M. J.; Greenhalgh, D. A.; Jenny, S. N.; Knights, C. F. *Corros. Sci.* **1986**, *26*, 537.
(96) Chou, H.-h.; Fan, H. Y. *Phys. Rev. B* **1976**, *13*, 3924.
(97) Liao, P. C.; Huang, Y. S.; Tiong, K. K. *J. Alloy Compd.* **2001**, *317*−*318*, 98.
(98) Cynn, H.; Sharma, S. K.; Cooney, T. F.; Nicol, M. *Phys. Rev. B* **1992**, *45*, 500.
(99) Shebanova, O. N.; Lazor, P. *J. Raman Spectrosc.* **2003**, *34*, 845.
(100) Ohtsuka, T.; Guo, J.; Sato, N. *J. Electrochem. Soc.* **1986**, *133*, 2473.